

# Commensurability Effects in Hexagonal Antidot Lattices with Large Antidot Diameters

S. Meckler and T. Heinzel\*  
*IPkM, Heinrich-Heine-Universität,  
 Universitätsstr.1, 40225 Düsseldorf, Germany*

A. Cavanna, G. Faini, U. Gennser, and D. Mailly  
*CNRS-LPN, Route de Nozay, 91960 Marcoussis, France*

(Dated: May 23, 2019)

The observation of a novel type of commensurability resonance in two-dimensional, hexagonal antidot lattices is reported. These resonances have a classical character and occur at large magnetic fields, typically above the resonance that corresponds to the cyclotron motion around a single antidot. The resonances are visible only for antidots with effective diameters larger than 50 % of the lattice constant. Simulations reveal that they originate from quasi-stable electron trajectories that bounce between three neighboring antidots. This interpretation is backed by the observation of large-period Aharonov-Bohm type oscillations at low temperatures.

PACS numbers: 73.23.-b, 73.63.-b

## I. INTRODUCTION

The study of electron transport in artificial, two-dimensional periodic potentials has revealed a variety of interesting phenomena over the past 15 years. One variant of such systems are antidot lattices, i.e. periodic potentials with maxima above the Fermi energy of the two-dimensional electron gas (2DEG) [1, 2, 3]. Most strikingly, resonances in the longitudinal magnetoresistance are found, which can be interpreted in terms of classical cyclotron orbits that are commensurate with the antidot lattice [2]. A more thorough classical treatment based on the Kubo formalism [4] has revealed that these resonances actually have their origin in the magnetic field dependent mixture of chaotic and regular trajectories, where the latter remain pinned in weak electric fields. Moreover, this theory provides an explanation for the observation of a negative Hall effect in weak magnetic fields  $B$  [5]. Another striking effect is the occurrence of  $B$ -periodic oscillations, which have been explained within a semiclassical theory of a few yet dominant quantized periodic orbits [6, 7]. More recently, signatures of the famous fractal energy spectrum of such potentials, also known as the Hofstadter butterfly, have been observed [8, 9].

A large fraction of these studies was performed on square [1, 2, 3, 6, 8, 9] or rectangular [10] lattices, while only a few experiments on hexagonal lattices have been published [11, 12, 13, 14]. For the majority of the effects, the lattice type is, in principle, irrelevant. Nevertheless, hexagonal lattices show some peculiarities that are absent in other types of antidot lattices. In particular, Altshuler-Aronov-Spivak oscillations have

been observed around  $B = 0$  in hexagonal lattices [12, 14], while Aharonov-Bohm oscillations can be detected at larger magnetic fields [13, 14]. Also, it has been suggested recently that scattering centers with a short range hexagonal order may be responsible for a phenomenology resembling that one observed in metal-insulator transitions in two dimensions [15]. Moreover, a detailed understanding of the transport in two-dimensional hexagonal lattices is of broad relevance, since this type of lattice is formed via self-organization on a mesoscopic scale in a variety of systems, such as vortex lattices in type II - superconductors [16] or in diblock copolymers [17].

Here, we report the observation of a novel type of magnetotransport resonances in hexagonal antidot lattices with large effective antidot diameters  $d_e \geq 0.5a$ , where  $a$  denotes the lattice constant. These resonances occur at cyclotron radii smaller than the antidot radius. Their signatures are visible only in the longitudinal component of the magneto-resistivity tensor, while temperature dependent measurements indicate a classical origin. Furthermore, Aharonov-Bohm type oscillations are observed at low temperatures that correspond to enclosed areas much smaller than the size of a lattice unit cell. These resonances are therefore attributed to quasi-stable trajectories which are localized in between three neighboring antidots. Numerical simulations of the magnetoresistivity based on the Kubo formalism support this interpretation and allow us to specify the characteristic trajectories.

The paper is organized as follows. In Section II, the sample preparation and the experimental setup is discussed. Section III is devoted to the experimental characterization of the resonances. In Section IV, we present numerical simulations and identify the relevant trajectories. A summary and conclusion is given in Section V.

---

\*Electronic address: thomas.heinzel@uni-duesseldorf.de

## II. SAMPLE PREPARATION AND EXPERIMENTAL SETUP

Conventional modulation doped  $GaAs/Al_{0.2}Ga_{0.8}As$  - heterostructures with an electron density of  $n = 2.5 \times 10^{15} \text{m}^{-2}$  and a carrier mobility of  $90 \text{m}^2/\text{Vs}$ , corresponding to an elastic mean free path of  $7.6 \mu\text{m}$  and to a Drude scattering time of  $\tau = 35 \text{ps}$  at liquid helium temperatures, have been grown by molecular beam epitaxy. A two-dimensional electron gas (2DEG) is located  $83 \text{nm}$  below the surface. A standard Hall bar geometry has been defined by optical lithography and wet chemical etching. The 2DEG is accessed electrically via  $Ni/AuGe$  Ohmic contacts. The hexagonal antidot arrays have been patterned by electron beam lithography and subsequent ion beam etching. The etch depth was  $50 \text{nm}$ . All antidot arrays have a lattice constant of  $600 \text{nm}$ , while lithographic antidot diameters of  $d_l = 100 \text{nm}$ ,  $200 \text{nm}$  and  $320 \text{nm}$  have been patterned. The measured array area was  $50 \mu\text{m} \times 25 \mu\text{m}$ .

Transport experiments have been carried out in a helium gas flow cryostat with a variable temperature insert and a superconducting magnet with a maximum field of  $B = 8 \text{T}$ , which is applied perpendicular to the plane of the 2DEG. The temperature has been varied from  $1.6 \text{K}$  to  $24 \text{K}$  with an accuracy of  $0.1 \text{K}$ . For measurements at lower temperatures, a top loading dilution refrigerator with a base temperature of  $80 \text{mK}$  has been used. AC current (frequency  $33 \text{Hz}$ , amplitude  $5 \text{nA}$ ) was passed through the antidot array. The longitudinal ( $\rho_{xx}$ ) and Hall ( $\rho_{xy}$ ) components of the resistivity tensor have been determined from voltage differences measured in the corresponding four-probe setups.

## III. EXPERIMENTAL RESULTS

Fig. 1 shows the measurements of  $\rho_{xx}$  as a function of  $B$  for arrays with a lattice constant of  $a = 600 \text{nm}$  and lithographic antidot diameters of  $d_l = 100 \text{nm}$ ,  $200 \text{nm}$ , and  $d_l = 320 \text{nm}$ . Due to lateral depletion of the 2DEG around the antidots of about  $100 \text{nm}$ , their electronic diameters  $d_e$  are larger. They can be estimated from the Shubnikov-de Haas oscillations observed in the antidot arrays, which give the Fermi wavelength in the array as well as, via their onset, the number of occupied transverse modes at the bottleneck formed by adjacent antidots. This way, effective electronic diameters of  $d_e \approx 300 \text{nm}$ ,  $400 \text{nm}$ , and  $550 \text{nm}$ , respectively, are found.

In the array with the smallest antidots (Fig. 1 (a)), typical commensurability oscillations in  $\rho_{xx}$  are found that, within the simple commensurability picture, in which the cyclotron diameter  $r_c = m^*v_F/(eB)$  matches the lattice constant in the resistivity maxima, can be attributed to orbits around 1, 3, and 7 antidots (numbers in Fig. 1(a)) [11], where the resonance around one antidot occurs at  $B = 270 \text{mT}$ . In comparison to the decay of the Shubnikov - de Haas oscillations with increasing

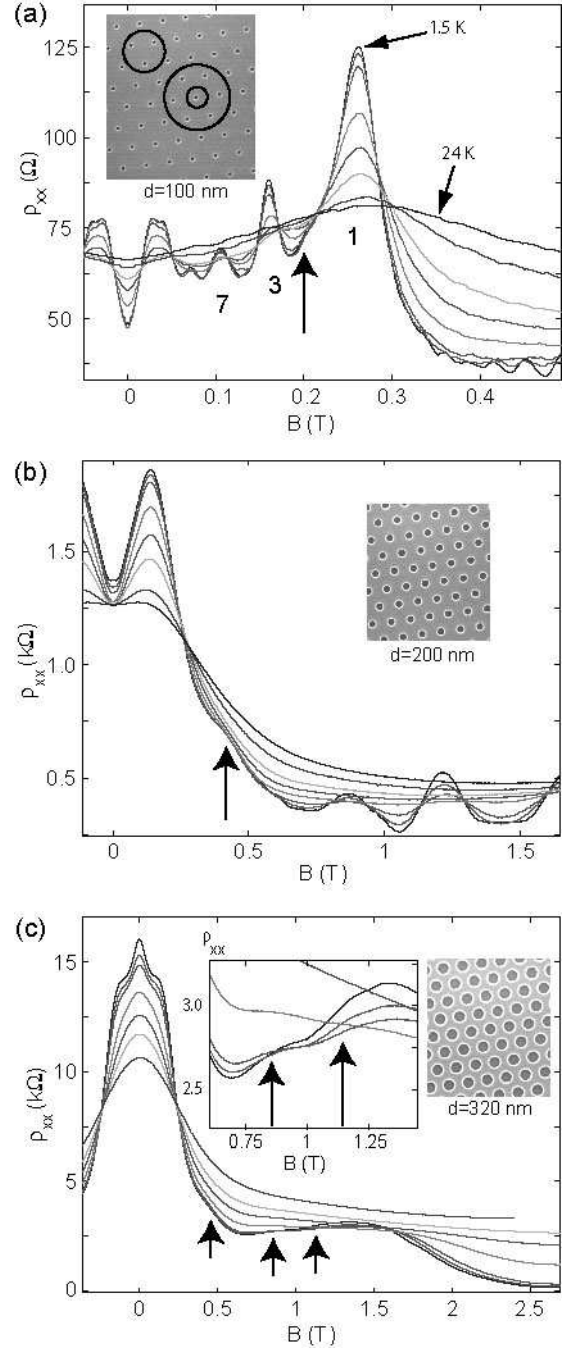


FIG. 1: Longitudinal magnetoresistivity of the hexagonal antidot arrays at temperatures of  $T = 1.5 \text{K}$ ,  $2.5 \text{K}$ ,  $4 \text{K}$ ,  $8 \text{K}$ ,  $12 \text{K}$ ,  $16 \text{K}$ , and  $24 \text{K}$ , as observed for arrays with  $a = 600 \text{nm}$  and different values of  $d_l$  (inset). In (a), the well known resonances corresponding to cyclotron orbits around 1, 3, and 7 antidots are observed. In (b) and (c), a known resonance is observed around  $B = 130 \text{mT}$ . The additional resonances are indicated by arrows. The inset in (c) shows a zoom-in from the main figure of the region of interest.

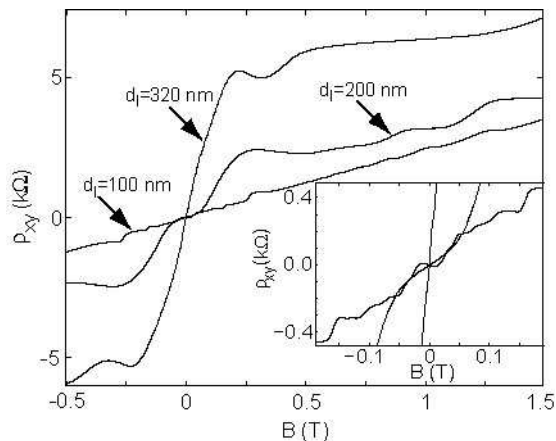


FIG. 2: Hall resistivities of the 3 arrays of Fig. 1, measured at  $T = 1.5\text{K}$ . In contrast to the conventional commensurability oscillations, the additional resonances cannot be identified. Note the negative Hall effect in the array with the small antidots (inset).

temperature, the temperature dependence of the commensurability oscillations is weak, which indicates their classical origin. Note that there is an additional weak shoulder at  $B = 200\text{mT}$  with a similar temperature dependence (vertical arrow in Fig. 1(a)).

Fig. 1 (b) shows the corresponding measurements on a sample with  $d_l = 200\text{nm}$ . Here, only one strong resonance with a classical character is visible at  $B = 130\text{mT}$ , which from the simulations described below can be attributed to a superposition of the commensurability oscillations identified in Fig. 1 (a). In addition, a weak resonance is observed at  $B = 400\text{mT}$ . This resonance is clearly not related to the Shubnikov - de Haas oscillations that set in around  $B = 0.6\text{T}$  and shows a different temperature dependence. A similar structure is observed in an array with  $d_l = 250\text{nm}$  (not shown). Moreover, in Fig. 1 (b), small features are observed between  $B = 0.5\text{T}$  and  $0.7\text{T}$  which, however, cannot be clearly distinguished from Shubnikov - de Haas oscillations. A similar pattern is observed in arrays with even larger antidot diameters, Fig. 1 (c). Here, three resonances, superimposed on a Shubnikov - de Haas resonance, are detected at  $B \approx 0.45\text{T}$ ,  $0.87\text{T}$ , and  $1.15\text{T}$ , respectively. These resonances are the main focus of the present paper.

The corresponding Hall measurements are shown in Fig. 2. While the structure of the conventional commensurability oscillations is reflected in  $\rho_{xy}(B)$ , no signatures of the novel resonances are detected here.

To obtain further insight into the character of these structures, we have studied the magnetotransport of the array with  $d_l = 320\text{nm}$  in a dilution refrigerator, see Fig. 3. Around  $B = 0$ , the well-known Altshuler-Aronov-Spivak oscillations with a period of  $\delta B = 8\text{mT}$  are observed (not shown) [12], which evolve into quasi-periodic Aharonov-Bohm type oscillations with a period of  $\delta B = 16\text{mT}$  for  $B > 60\text{mT}$ . The Aharonov-Bohm pe-

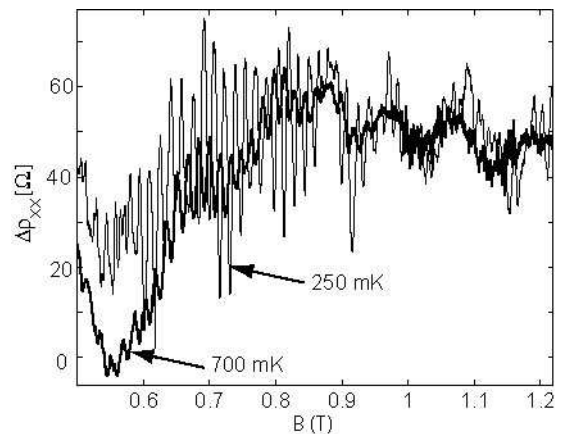


FIG. 3: Magnetoresistivity of the array with  $d_l = 320\text{nm}$  as measured in the dilution refrigerator, as observed in the magnetic field regime of the novel resonances. A smooth background has been subtracted. Here, the quasi-periodic Aharonov-Bohm oscillations are modulated with a period of  $\delta B \approx 120\text{mT}$ .

riod corresponds to a characteristic area of  $A = h/e\delta B = 2.6 \times 10^{-13}\text{m}^2$ , in rough agreement with the area of a lattice unit cell ( $A_{\text{cell}} = 3.1 \times 10^{-13}\text{m}^2$ ). This evolution has been reported and interpreted previously [13]. An additional, superimposed oscillation, however, with a period of  $\delta B \approx 120\text{mT}$  is observed in the magnetic field regime where the novel classical resonances are detected. Interpreting this oscillation in terms of an Aharonov-Bohm effect, the enclosed area corresponds to about 11% of a unit cell, i.e.  $A \approx 3.4 \times 10^{-14}\text{m}^2$ . All periodic oscillations smear out as the temperature is increased with the amplitude decaying roughly  $\propto 1/T$ ; the oscillation with the larger period persists to higher temperatures.

#### IV. INTERPRETATION AND DISCUSSION

We interpret our results in terms of commensurability oscillations that exist in the open electron pockets formed in between three adjacent antidots. Quasi-stable orbits may form by consecutive reflections of the electrons at the antidot walls. It is plausible that such trajectories would become more stable as  $d_e/a$  increases. We determine the characteristic area of such a pocket from  $A_{\text{pocket}} = \frac{1}{2}(A_{\text{cell}} - \pi(d_e/2)^2)$  and estimate in our large antidot array to  $A_{\text{pocket}} \approx 3.6 \times 10^{-14}\text{m}^2$ , i.e., significantly smaller than the area of the unit cell. Hence, an increased Aharonov-Bohm period can be expected, although the exact period depends on the details of the closed trajectory, as well as on the steepness of the antidot walls.

In order to substantiate this interpretation, we have performed model calculations based on the Kubo formalism [18]. The antidot lattice is modelled by a two-dimensional, hexagonal array of hard-wall cylinders of the estimated electronic diameter  $d_e$  in the samples of

Fig. 1. For each value of  $B$ ,  $10^5$  electrons with a fixed Fermi energy adapted to the experimental conditions ( $E_F = 8.86\text{meV}$ ) are injected at random positions and with random velocity directions within a unit cell of the lattice in a magnetic field. Their trajectories are calculated to a length of  $50\mu\text{m}$ , corresponding to a time of flight of  $240\text{ps}$ . The electron velocity correlation functions  $v_i(t, B)v_j(0)$  are calculated and averaged over all trajectories. Within the Kubo formalism, the components of the magneto-conductivity tensor are obtained for a degenerate two-dimensional electron gas from

$$\sigma_{ij}(B) = \frac{m^*e^2}{\pi\hbar^2} \int_0^\infty \langle v_i(t, B)v_j(0) \rangle e^{-t/\tau} dt \quad (1)$$

In Eq. (1),  $m^* = 0.067m_e$  is the effective electron mass in GaAs. The brackets denote averaging over all trajectories [19]. Elastic scattering due to random impurities is taken into account via the exponential cutoff function that appears in the integrand. Here, a Drude scattering time of  $\tau = 35\text{ps}$  has been chosen, in accordance with the mobility of the pristine 2DEG. This model is a simplified version of the more thorough treatment presented in Ref. [4]. In particular, neither the driving electric field nor the finite slope of the antidot walls are taken into account. Nevertheless, our simplified model allows us to identify the trajectories that generate the additional resonances. In Fig. 4, the results of the simulated  $\rho_{xx}(B)$  for the three arrays under study are reproduced. For the largest antidots ( $d_e = 550\text{nm}$ ), pronounced resistivity minima are found around  $B = 0.78\text{T}$ ,  $1.4\text{T}$ , and  $1.85\text{T}$ , while the commensurability resonance around a single antidot is barely visible at  $B \approx 0.3\text{T}$ .

To gain more insight into the origin of these structures, we have taken Poincaré sections along the perpendicular bisector of the line connecting the centers of two neighboring antidots, see Fig. 5. As the magnetic field increases to  $B = 0.6\text{T}$ , stable regions emerge with a structure as shown in in Fig. 5 (a), with an areal fraction in the Poincaré sections that peaks around the minimum in  $\rho_{xx}$  at  $B = 0.78\text{T}$ . Around the resistivity maximum at  $1\text{T}$ , this pattern fades and evolves into a second one shown in Fig. 5(b), which is most pronounced around the minimum at  $1.4\text{T}$ . At larger magnetic fields, the stable regions gradually fade until they can no longer be identified. We pick the Poincaré sections at  $B = 0.6\text{T}$  and at  $B = 1.2\text{T}$  for a detailed discussion. In both cases, stable regions are found which contain two types of trajectories depicted to the right of Figs. 5 (a) and (b), respectively. The first type, labelled by **1** in Fig. 5, consists of skipping orbits around an individual antidot. This type is present for all magnetic fields above  $0.5\text{T}$  and covers a continuously increasing area in the Poincaré section as  $B$  is increased up to  $2\text{T}$ . The second type of trajectories are triangularly shaped and form quasi-closed figures by consecutive reflections at walls of adjacent antidots. They have been classified by

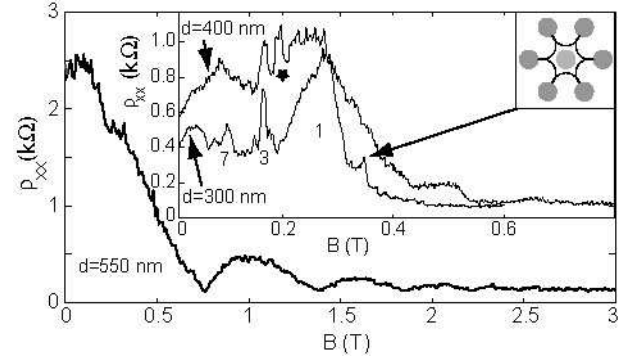


FIG. 4: Simulated longitudinal magnetoresistivity of the array with  $d_e = 550\text{nm}$ . Weak resonances are found in  $0.6\text{T} \leq B \leq 2.2\text{T}$ . The inset shows the corresponding simulations for the arrays with  $d_e = 300\text{nm}$  and  $d_e = 400\text{nm}$ . Here, the star denotes an unidentified resonances, while the cartoon to the upper right sketches the type of trajectory found in the feature indicated by the arrow.

the number of consecutive bounces at the same antidot wall before moving on to an adjacent antidot, and are labelled in Fig. 5 by **2** and **3**, respectively. This type is present in both types of Poincaré sections, although with a smaller areal fraction in the Poincaré sections at larger magnetic fields. Trajectories with two consecutive bounces at the same wall are present only for  $B > 1\text{T}$ . Since the skipping orbits (type 1) are present not only at all magnetic fields with a smoothly varying weight in the Poincaré sections, but also in other antidot lattice types, they most likely do not cause the resonance pattern. The weight of the type 2 trajectories, however, shows broad maxima around  $0.7\text{T}$  and  $1.2\text{T}$ . Hence, we attribute the structure in the resistivity of the array with the large antidots to the triangular or rosette - shaped trajectories whose weight depends on the magnetic field. They are most important around the minima of  $\rho_{xx}$ , which is counter-intuitive at first thought. This, however, is a consequence of the large magnetic field, since localized states that generate a minimum in  $\sigma_{xx}(B)$  translate into a minimum in  $\rho_{xx}(B)$  for  $\rho_{xy} \gg \rho_{xx}$ , which is the case here. Thus, a second characteristic feature of the novel commensurability resonances which distinguishes them from those known previously is the fact that the magnetic field at which the quasi-stable trajectories are most pronounced correspond to a minimum in  $\rho_{xx}$ . Similar simulations for the arrays with smaller antidot diameters are shown in the inset of Fig. 4. The structure measured in the array with  $d_l = 100\text{nm}$  is fairly well reproduced by a simulation with  $d_e = 300\text{nm}$ . In addition, a peak around  $0.35\text{T}$  is obtained in the simulations, which is not observed in the experiment. It can be attributed to the trajectory sketched in the inset. This trajectory may be too unstable to be observable, or it may be strongly modified by soft walls. Furthermore, the resonance around one antidot has a wing extending to small magnetic fields. A characteristic trajectory for this

wing could not be identified, since the Poincaré sections do not show stable regions besides those corresponding to the commensurability resonance around one antidot. Hence, the origin of the shoulder at 0.2T in Fig. 1(a) cannot be attributed to a characteristic trajectory. This is also the case for the peak denoted by a star in the simulation for  $d_e = 400\text{nm}$  (see the inset in Fig. 4). Note that in the simulations for this array, the resonances at large magnetic fields begin to emerge already.

In these numerical studies, we do not observe any signature of the quasi-localized states at large magnetic fields in the Hall resistance (not shown). This is in agreement with the experimental observations, and is probably due to the fact that their contribution to  $\rho_{xy}$  is too small to be observed, in contrast to the commensurability effects at smaller fields, which are clearly visible in  $\rho_{xy}$ , see Fig. 2.

In comparison to the experiments, we are led to the conclusion that commensurability resonances residing in between adjacent antidots are causing the structure measured in the resistivity. Quantitative deviations remain, and not all of the observed structures could be identified. In particular, the areas enclosed by the simulated trajectories are much smaller than those of the electron pockets. A quantitative agreement, however, should not be expected, due to the limitations of our model. We expect that by inclusion of a more realistic potential landscape and of the driving electric field along the lines of ref. [4], the agreement could be improved.

## V. SUMMARY AND CONCLUSION

In summary, we observe novel resonances in hexagonal antidot lattices with large antidot diameters. Classical simulations suggest that they can be attributed to classical, quasi-periodic trajectories of various shapes that are caught in between three adjacent antidots. This interpretation is supported by measurements at 250mK, where the samples show Aharonov-Bohm oscillations with a characteristic area similar to that one of an electron pocket in between antidots. It remains to be seen whether such resonances are also visible in other types of antidot lattices. In addition, it would be interesting to perform more sophisticated simulation with more realistic potential landscapes, and study the stability of the triangular- and rosette-type trajectories in the presence of additional driving electric fields.

Financial support by the *Heinrich-Heine-Universität*

*Düsseldorf* and by the *Region Ile de France* and the *Conseil Général de l'Essonne* is gratefully acknowledged. The authors acknowledge technical support by Ch. Dupuis.

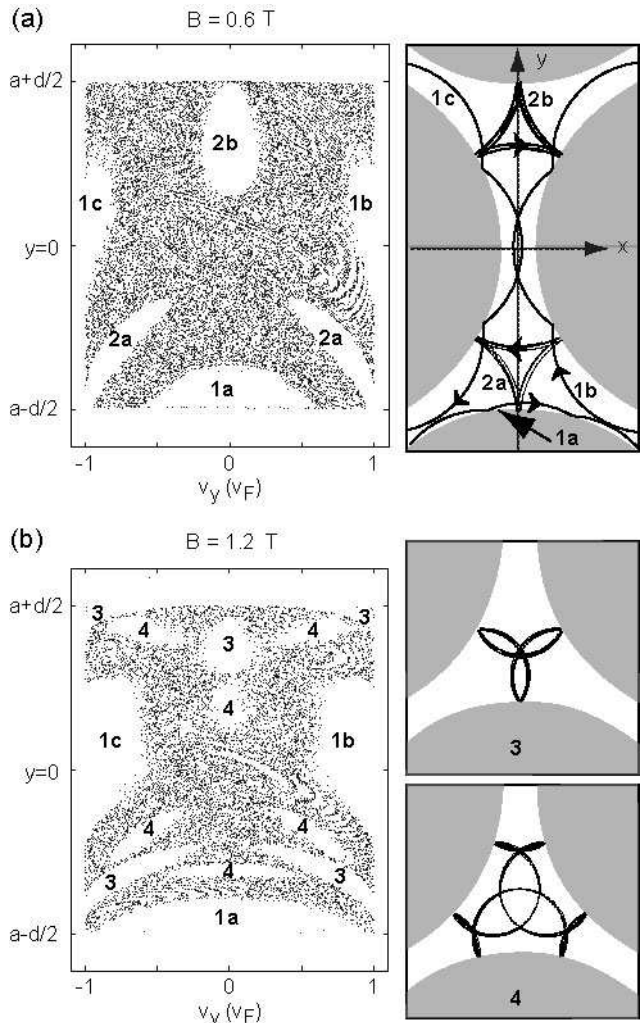


FIG. 5: Poincaré - sections (left) taken from the array with  $d_e = 550\text{nm}$  at  $B = 0.6\text{T}$  (a) and  $1.2\text{T}$  (b). The sections are taken along the  $y$ -direction at  $x = 0$ , see the right part of (a), where the gray areas denote the antidots. The characteristic trajectories (right) found in the stable regions are assigned according to the numbers in the stable regions, see text. Note that only the intersections of the trajectories with  $v_x > 0$  are plotted in the Poincaré - sections.

- [1] K. Ensslin and P. M. Petroff, Phys. Rev. B **41**, 12307 (1990).
- [2] D. Weiss, M. L. Roukes, A. Menschig, P. Grambow, K. v. Klitzing, and G. Weimann, Phys. Rev. Lett. **66**, 2790 (1991).

- [3] A. Lorke, J. P. Kotthaus, and K. Ploog, Phys. Rev. B **44**, 3447 (1991).
- [4] R. Fleischmann, T. Geisel, and R. Ketzmerick, Phys. Rev. Lett. **68**, 1367 (1992).
- [5] R. Fleischmann, T. Geisel, and R. Ketzmerick, Europhys.

- Lett. **25**, 219 (1994).
- [6] D. Weiss, K. Richter, A. Menschig, R. Bergmann, H. Schweizer, K. v. Klitzing, and G. Weimann, Phys. Rev. Lett. **70**, 2793 (1993).
  - [7] K. Richter, Europhys. Lett. **29**, 7 (1995).
  - [8] C. Albrecht, J. H. Smet, K. v. Klitzing, D. Weiss, V. Umansky, and H. Schweizer, Phys. Rev. Lett. **86**, 147 (2001).
  - [9] T. Schlösser, K. Ensslin, J. P. Kotthaus, and M. Holland, Europhys. Lett. **33**, 683 (1996).
  - [10] R. Schuster, K. Ensslin, J. P. Kotthaus, M. Holland, and C. Stanley, Phys. Rev. B **47**, 6843 (1993).
  - [11] D. Weiss, K. Richter, E. Vasiadou, and G. Lütjering, Surf. Sci. **305**, 408 (1994).
  - [12] F. Nihey, S. W. Hwang, and K. Nakamura, Phys. Rev. B **51**, 4649 (1995).
  - [13] M. Ueki, A. Endo, S. Katsumoto, and Y. Iye, Physica E **22**, 365 (2004).
  - [14] Y. Iye, M. Ueki, A. Endo, and S. Katsumoto, J. Phys. Soc. Japan **73**, 3370 (2004).
  - [15] T. Heinzel, R. Jäggi, E. Ribeiro, M. v. Waldkirch, K. Ensslin, S. Ulloa, G. Medeiros-Ribeiro, and P. M. Petroff, Europhys. Lett. **61**, 674 (2003).
  - [16] M. Tinkham, *Introduction to Superconductivity* (Dover Books on Physics, 2004).
  - [17] T. Thurn-Albrecht, J. Schotter, G. Kastle, N. Emley, T. Shibauchi, L. Krusin-Elbaum, K. Huarini, C. T. Black, M. T. Touminen, and T. P. Russell, Science **290**, 2126 (2000).
  - [18] R. Kubo, J. Phys. Soc. Jpn. **12**, 570 (1957).
  - [19] K. Richter, *Semiclassical theory of mesoscopic quantum systems* (Springer, 2004).